Corrosion Science 147 (2019) 384–393

Contents lists available at ScienceDirect

Corrosion Science

journal homepage: www.elsevier.com/locate/corsci

Corrosion behaviour of WC hardmetals with nickel-based binders

A.M. Ferro Rocha[a], A.C. Bastos[a,*], J.P. Cardoso[a], F. Rodrigues[b], C.M. Fernandes[a], E. Soares[b], J. Sacramento[b,c], A.M.R. Senos[a], M.G.S. Ferreira[a]

[a] University of Aveiro, Department of Materials and Ceramic Engineering, CICECO - Aveiro Institute of Materials, 3810-193, Aveiro, Portugal
[b] DURIT – Metalurgia Portuguesa do Tungsténio, Lda., Arruamento C – Zona Industrial, 3854-909, Albergaria-a-Velha, Portugal
[c] ESTGA – Escola Superior de Tecnologia e Gestão de Águeda, Universidade de Aveiro, Rua Comandante Pinho e Freitas, 3750-127, Águeda, Portugal

ARTICLE INFO

Keywords:
Hardmetals
WC
Metal matrix composites
EIS

ABSTRACT

Cobalt is the standard binder in tungsten carbide (WC) hardmetals due to its compatibility with the WC phase, resulting in composites with exceptional hardness and wear resistance. However, their corrosion resistance is not satisfactory in many applications, leading to the early deterioration and failure of tools and equipment.

In this work, the corrosion of WC hardmetals with three alternative binders (FeCoNi, NiCrCoMo and NiCrMo) is compared with a benchmark WC-Co composite, using electrochemical techniques such as open circuit potential (OCP) monitoring, polarisation curves and electrochemical impedance spectroscopy (EIS), assisted by scanning electron microscopy (SEM).

1. Introduction

Due to the remarkable hardness and wear resistance, hardmetals were introduced to the industry in the first half of the 20th century as substitutes for diamond in drawing dies [1]. Hardmetals are known for having a brittle phase (WC) with high hardness, and a binder phase (typically Co) that confers ductility to the composite. Cobalt is the standard binder for hardmetals, owing to its excellent wettability on WC grains, making it possible to produce dense sintered materials with high hardness and good fracture toughness [2]. In addition, the wide knowledge on cobalt magnetic and electrical properties, enables non-destructive and high accuracy quality control of the produced grades [2,3]. The mechanical properties allow the use of WC-Co in a vast range of applications where abrasion and wear are of major concern. Examples are valves for pumping systems, drawing dies, extrusion dies, saw blades, metal forming tools, drill bits for rock, bearing tools, flux-cored wire tools, and more [2,4]. All these tools find application in the mining, chemical, oil and gas industries, among others. Despite the outstanding properties, the WC-Co system has been associated with health concerns [5] and faces supply uncertainties related to ore extraction [6,7]. In service, hardmetals can contact aqueous environments with variable pH, salinity and oxygen concentration [4,8–11].

Iron and nickel based binders have been studied for the substitution of Co, as they allow the production of ductile and dense composites, with mechanical properties comparable to common WC-Co grades [6,12–14]. The use of more complex binder systems (with various alloying elements) has also been reported, some of them having similar or even better characteristics than WC-Co [12,14–18].

In our group, extensive work on the Co replacement in hardmetals has been undertaken, and AISI304 stainless steel has proved to be a valid alternative [7,19–22]. It was possible to produce composites with increased hardness and toughness when compared to WC-Co, although with no significant improvement in corrosion resistance. This time, composites with complex metallic binders – WC-FeCoNi, WC-NiCrCoMo and WC-NiCrMo – were produced. Similar compositions have been studied [2,12,14,22–24] and were able to match the properties achieved by conventional hardmetal grades. At certain elemental ratio, the FeCoNi binder revealed mechanical properties comparable to WC-Co [2,6]. In small additions to the binder, Mo ensures a refinement of the WC grains, which leads to an increase of both hardness and wear resistance [25]. Good mechanical properties compared to WC-Co were also found for the WC-NiCrMo system [26]. While the mechanical properties have been widely investigated, less attention has been devoted to the corrosion resistance of these materials. In this work, the corrosion of the synthesised WC-FeCoNi, WC-NiCrCoMo and WC-NiCrMo was studied in 0.5 M NaCl and compared to a WC-Co benchmark, using electrochemical techniques, such as open circuit potential (OCP) monitoring, current-potential curves and electrochemical impedance spectroscopy (EIS), with the help of SEM analysis.

* Corresponding author.
E-mail address: acbastos@ua.pt (A.C. Bastos).

https://doi.org/10.1016/j.corsci.2018.11.015
Received 1 February 2018; Received in revised form 13 November 2018; Accepted 18 November 2018
Available online 26 November 2018

Table 1
Nominal compositions of the produced composites.

	WC content		Binder content		Binder composition (% wt.)				
	(% wt.)	(% vol.)	(% wt.)	(% vol.)	Co	Fe	Ni	Cr	Mo
WC-Co	88	82 ± 1	12	18 ± 1	100				
WC-FeCoNi	90		10		20	40	40		
WC-NiCrCoMo	90		10		15		70	11	4
WC-NiCrMo	90		10				83	11	6

2. Experimental

2.1. Materials

The composites were produced with powders of WC, Cr_3C_2 and FeCoNi from H.C. Starck GmbH (Germany), Co (Umicore, Belgium), Ni (A.M.P.E.R.E. Industrie SASU, France) and Mo_2C (Treibacher Industrie AG, Austria), with average particle size ranging between 1 and 1.5 μm. The nominal compositions are presented in Table 1. The binder content was chosen according to the rule of mixtures [27] to be ~ 18 % vol. in all composites. All specimens were produced according to standard powder metallurgy routes, where the WC powder was mixed and milled together with the as-proportioned binder powders in a rotatory ball mill for 65 h, at 90 rpm, using ethanol as the milling media. Ni based powders needed longer milling times (72 h) to achieve the desired final particle size. The formulations were dried and uniaxially pressed (50 MPa), followed by a 12 h sintering cycle in an industrial sinter-HIP furnace at maximum temperatures of 1400 to 1500 °C during 1.5 h and 3 MPa of applied pressure.

2.2. Structural and microstructural characterization

Optical microscopy (Leica DM LM) was used to determine the porosity (according to ISO 4505) and to check for defects and for the presence of the η-phase or free carbon on the samples microstructures. Prior to the observations, the sintered compacts were polished with diamond paste up to a 3 μm finish followed by chemical etching using Murakami's solution (10 g potassium ferricyanide and 10 g sodium hydroxide in 100 ml distilled water). Scanning Electron Microscopy (SEM) was performed in a Hitachi SU-70 microscope with an accelerating voltage of 15 kV at a distance from the tip of 15 mm. WC average grain sizes were determined with the Image J software [28] based on SEM images with a minimum of 300 grains per picture. XRD diffraction patterns were collected in a Rigaku diffractometer, with 2θ steps of 0.02° and 100 s of acquisition time.

2.3. Mechanical properties

Density, hardness and fracture toughness were determined. The density was measured by the Archimedes' principle, the hardness (HV30) by Vickers indentation (Zwick/Roell ZHU) and the fracture toughness was determined in accordance with the Palmqvist method, using the equation proposed by Shetty et al. [29],

$$K_{IC} = A\sqrt{H}\sqrt{\frac{P}{\sum l}} \quad (1)$$

where H stands for hardness (Pa), P is the applied load (N), Σ l is the sum of the crack lengths (m) and A is a constant with the value of 0.0889. For each composite two specimens were tested with five indentations per specimen.

2.4. Corrosion measurements

The samples were electrically connected from the back and mounted in epoxy resin, so that only one side was in contact with the electrolyte solution. All samples were ground with diamond discs of decreasing granulometry, from 75 μm to 18 μm, and finally rinsed with distilled water followed by ethanol. Insulating tape (Scotch 3 M) was used to delimit the working area of each sample (area = 0.24 cm^2). Polarisation curves, EIS (electrochemical impedance spectroscopy) and open circuit potential (OCP) were measured with a PGSTAT302 N Potentiostat (Autolab Metrohm). All experiments were performed in electrochemical cells with a three-electrode arrangement, consisting of the working electrode (resin mounted sample), a platinum counter electrode and a saturated calomel electrode (SCE) as reference. The measurements were performed in 0.5 M NaCl aqueous solution, prepared with pro analysis grade reagent (Alfa Aesar) and distilled water, inside a Faraday cage, at room temperature (23 ± 2 °C) and open to air. The OCP was continuously monitored during the first 24 h of immersion. The polarisation curves were obtained 1 h after immersion with a scan rate of 0.2 mV s^{-1} and 1 mV s^{-1} for the anodic and cathodic branches, respectively. EIS measurements were done at open circuit potential, with a 10 mV (rms) sinusoidal perturbation in the 100 kHz to 1–10 mHz frequency range and ten points per frequency decade. Experiments were done in triplicate.

3. Results and discussion

3.1. Samples characterization

3.1.1. Structural and microstructural analysis

The microstructure of each composite after polishing and chemical etching is presented in Fig. 1. The WC grains appear as lighter areas, surrounded by the binder phase (darker areas). The microstructures are homogeneous, with the WC grains well dispersed in the binder, and almost no porosity (Table 2). It also becomes clear that the carbides Cr_3C_2 and Mo_2C (added as precursors for the metallic elements Cr and Mo), completely dissolved in the binder without giving rise to secondary phases. Free carbon and η-phase were not detected. The XRD spectra shown in Fig. 2 support the microstructural analysis since the WC phase is present in every spectra (peaks of higher intensity) along with the binder related phases. The binder peaks are dominated by the element(s) in greater amount of each alloy, Fe (α) and FeNi in FeCoNi, and Ni in NiCrCoMo and in NiCrMo. The other metallic elements dissolve in the matrix, integrating its structure and not giving individualised signal.

3.1.2. Physical properties

Table 2 presents the results of the mechanical testing, namely hardness and fracture toughness. The lowest hardness was measured on WC-FeCoNi followed by WC-Co, whereas higher values were found on WC-NiCrCoMo and WC-NiCrMo. WC-Co presented the highest K_{IC}. The values of the other composites were lower but still inside the acceptable range for hardmetals [30]. WC-NiCrCoMo was the only composite with traces of porosity, but the hardness is still better than that of WC-Co and WC-FeCoNi. All produced samples possess micrometric or sub micrometric grains which is directly related to the mechanical properties – smaller grain size is typically associated with higher hardness [2,31–33]. The presence of Mo and Cr in both WC-NiCrCoMo and WC-NiCrMo resulted in the reduction of the average grain size. This

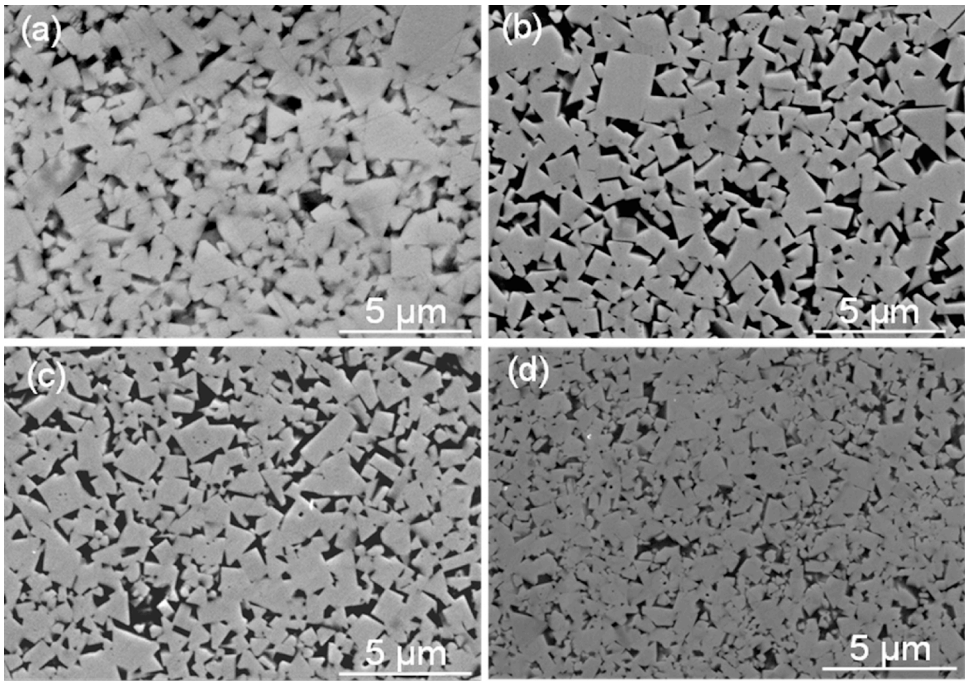

Fig. 1. SEM images of polished surfaces etched with Murakami's solution: (a) WC-Co; (b) WC-FeCoNi; (c) WC-NiCrCoMo and (d) WC-NiCrMo.

reduction was more evident in the case of WC-NiCrMo and is related with the absence of Co in this sample, which is known to promote WC grain growth [34].

3.2. Corrosion evaluation

3.2.1. Open circuit potential monitoring

The corrosion potential (E_{corr}) of the composites in 0.5 M NaCl was measured for the first 24 h of immersion and is plotted in Fig. 3. In the first hour of immersion the new composites exhibited potentials more positive than WC-Co. After 24 h of immersion, WC-FeCoNi presented the lowest potential, slightly more negative than WC-Co, while the potentials of the other two composites, WC-NiCrCoMo and WC-NiCrMo, were 400 mV more positive.

3.2.2. Polarisation curves

Fig. 4 shows the current density-potential curves of the four systems, measured after 1 h of immersion in 0.5 M NaCl. The anodic branches (Fig. 4 a) reveal active response of WC-Co and WC-FeCoNi, evidenced by the fast increment in current as the potential becomes more positive. On the contrary, the currents of the two other composites grow slowly, and only after 200 mV overpotential in WC-NiCrCoMo and 400 mV in WC-NiCrMo a sharp increase occurs. The different potentials at which the current rises sharply are more evident in the plot with the current density in linear scale, shown as inset.

The cathodic branches (Fig. 4 b) depict limiting plateaus for the oxygen reduction between -0.4 V_{SCE} and -0.9 V_{SCE}. This reaction is controlled by activation in WC-NiCrCoMo and WC-NiCrMo, and is diffusion controlled in WC-Co and WC-FeCoNi. All curves become dominated by the hydrogen evolution reaction at potentials more negative than -0.9 V_{SCE}.

Tafel extrapolation was used to determine the corrosion rates (i_{corr}), the corrosion potential E_{corr}, and the Tafel slopes (β_a and β_c), which are presented in Table 3. The lowest corrosion rates were obtained for WC-NiCrMo and WC-NiCrCoMo (~ 0.2 and 0.6 µA cm^{-2}, respectively) which are about one order of magnitude lower than for WC-Co and WC-FeCoNi. The polarisation resistance method was also employed and Fig. 5 presents the results of one set of experiments. The mean value of the polarisation resistance (R_p) obtained for WC-NiCrMo was 115.7 ± 54.8 kΩ cm^2, nearly three times higher than for WC-NiCrCoMo (38 ± 19.8 kΩ cm^2), and two orders of magnitude higher than the other two compositions (2.9 ± 0.8 kΩ cm^2 for WC-Co and 3.2 ± 2.3 kΩ cm^2 for WC-FeCoNi).

The R_p values were used to calculate i_{corr} according to the Stern-Geary equation [35,36],

$$i_{corr} = \frac{\beta_a \beta_c}{2.3(\beta_a + \beta_c)R_p} \quad (2)$$

with the β_a and β_c taken from Table 3. For the cases where the cathodic reaction was diffusion controlled ($\beta_c \rightarrow \infty$), a limit equation was used [36],

Table 2
Physical and mechanical properties of all composites.

	Density[a] (g cm^{-3})	Porosity[b]	G_{avg}[c] (µm)	Hardness (HV30)	K_{IC}[d] (MPa $m^{1/2}$)
WC-Co	14.30	A00B00C00	1.00	1420 ± 19	14.3 ± 0.7
WC-FeCoNi	14.12	A00B00C00	0.81	1369 ± 12	10.5 ± 0.3
WC-NiCrCoMo	14.21	A08B00C00	0.75	1495 ± 18	9.5 ± 0.2
WC-NiCrMo	14.33	A00B00C00	0.52	1577 ± 16	10.6 ± 0.2

[a] Apparent density.
[b] ISO 4505:1978.
[c] Average of WC grain size.
[d] Palmqvist method.

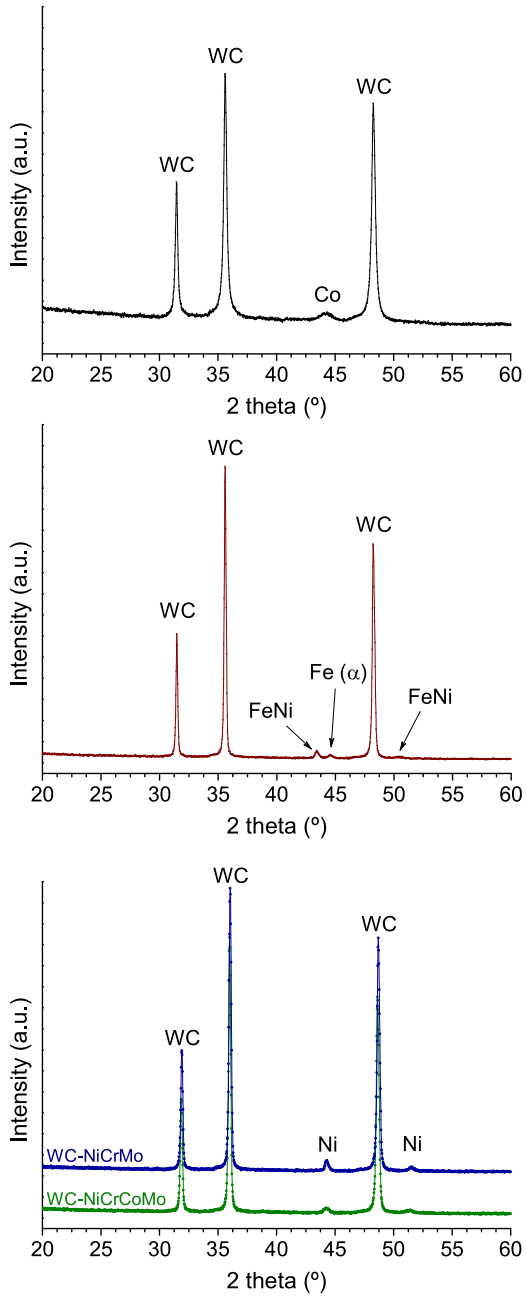

Fig. 2. XRD patterns of (a) WC-Co, (b) WC-FeCoNi, (c) WC-NiCrCoMo and WC-NiCrMo.

$$i_{corr} = \frac{\beta_a}{2.3R_p} \quad (3)$$

The i_{corr} values calculated from the R_p are nearly two times higher than those obtained from Tafel extrapolation, but the trend and the relative order of values remain the same.

3.2.3. Electrochemical impedance spectroscopy

The impedance spectra measured during two weeks of immersion in 0.5 M NaCl is presented in Fig. 6. In the first moments of WC-Co exposure to the test solution, only one time constant dominated the impedance response. During the first day of immersion, a second time constant appeared and, with time, the two responses became progressively separated in the frequency spectrum. Evidences of a third relaxation process, possibly due to diffusion of some species, appeared at the lower frequency range of a few spectra. The total impedance was

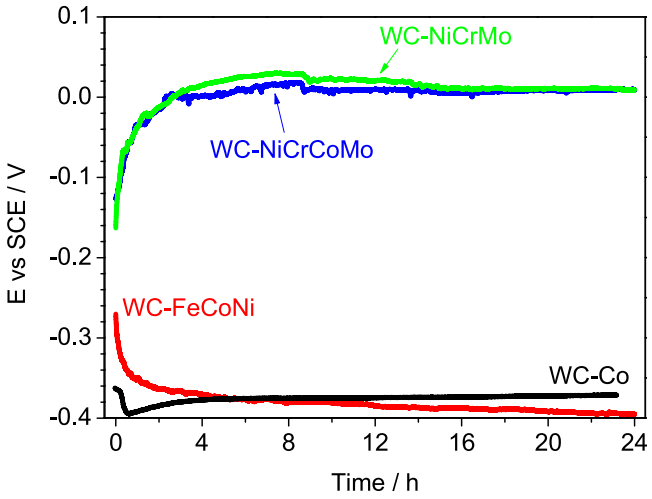

Fig. 3. Corrosion potential of the composites in the first 24 h of immersion in 0.5 M NaCl.

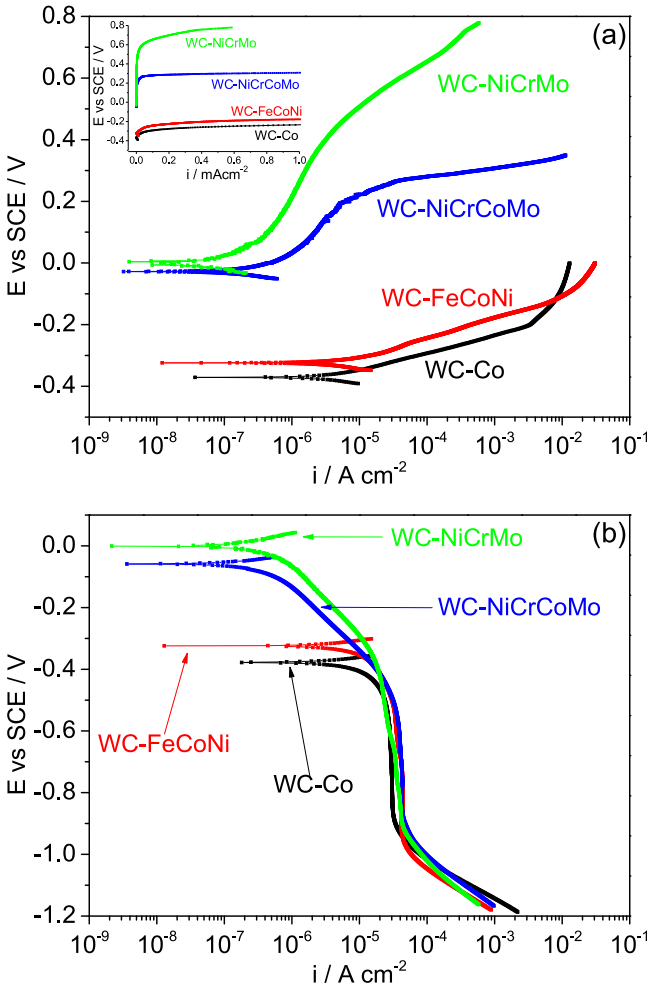

Fig. 4. Polarisation curves of the four composites after 1 h of immersion in 0.5 M NaCl: (a) anodic branches, (b) cathodic branches.

about 2×10^3 Ω cm^2 in the beginning of exposure, and increased 4 times in the 2 weeks testing period. The response of WC-FeCoNi followed the trend described for WC-Co, but the two time constants were already visible after 1 h of immersion and the total impedance dropped four times, from 4×10^3 Ω cm^2 to 10^3 Ω cm^2 in two weeks of immersion. The other two composites, WC-NiCrCoMo and WC-NiCrMo,

Table 3
Electrochemical parameters extracted from OCP and current-potential curves.

	E_{corr} (V_{SCE})		β_a (V dec^{-1})	β_c (V dec^{-1})	i_{corr} from Tafel extrapolation (μA cm^{-2})	i_{corr} from *Rp* (μA cm^{-2})
	OCP monitoring 24h	Polarisation curves 1h				
WC-Co	−0.343 ± 0.023	−0.397 ± 0.060	0.095 ± 0.036		6.03 ± 3.82	14.45 ± 6.80
WC-FeCoNi	−0.386 ± 0.007	−0.347 ± 0.086	0.050 ± 0.016		4.48 ± 3.19	6.87 ± 5.41
WC-NiCrCoMo	−0.052 ± 0.060	−0.098 ± 0.066	0.204 ± 0.105	−0.216 ± 0.010	0.56 ± 0.28	1.20 ± 0.63
WC-NiCrMo	−0.057 ± 0.049	−0.091 ± 0.070	0.393 ± 0.063	−0.194 ± 0.025	0.21 ± 0.18	0.49 ± 0.23

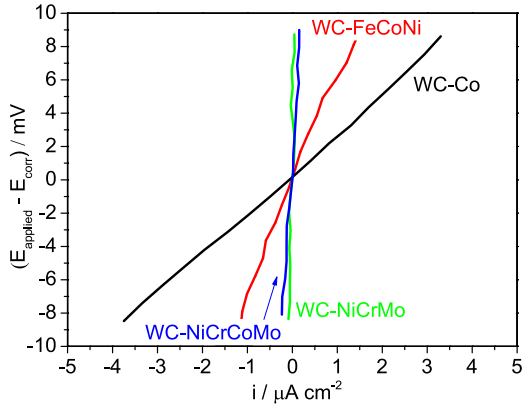

Fig. 5. Polarisation resistance measured in 0.5 M NaCl after 1 h in 0.5 M NaCl.

exhibited much higher impedance (nearly 10^6 Ω cm^2) with a capacitive response, typical of passive systems. Numerical fitting of the EIS spectra was performed with the ZView software (Scribner Associates, USA) using the equivalent electric circuit shown in Fig. 7. The results of the numerical fitting appear as lines in Fig. 6 while the symbols are experimental points. In the circuit, R_s is the uncompensated solution resistance, C_{HF} is the capacitive response of a surface layer with passive character, R_{HF} is the resistance of the solution inside the pores of the surface layer, C_{dl} and R_{ct} are, respectively, the double layer capacitance and the charge transfer resistance of the electrochemical processes (corrosion) occurring at the bottom of the pores. The impedance of the "passive" composites – WC-NiCrCoMo and WC-NiCrMo – could be fitted with a single time constant but a better fit was obtained with two time constants, one at higher frequencies due to the passive layer and another at lower frequencies related to the corrosion process in pores. The difference between the "active" and the "passive" composites is that, in the latter, the pores are much smaller and short lived, with corrosion being therefore much smaller.

In WC-Co and WC-FeCoNi, the time constant related to corrosion becomes more important as time of immersion elapses. Taking into account the microscopic inspection of the surfaces presented in the next section, it is possible that, at later stages, the equivalent circuit in Fig. 7 assumes the form of the circuit proposed in reference [21], where C_{HF} is the capacitance of the surface (including the double layer at the WC surface and the capacitive response of the layer of corrosion products), R_{HF} is the resistance of the solution inside the pits and C_{dl} and R_{ct} are related to the corrosion process in the pits. The corrosion evolves mainly underneath the surface with dissolution of the binder between the WC particles. According to the microscopic inspection presented in Section 3.2.4. and in agreement with the literature [4,21,26] the WC particles do not corrode in the testing conditions used in this work.

In the cases where diffusion manifested, a RC network was added in the equivalent circuit in series with R_{ct} (dashed box in Fig. 7) accounting for the resistive and capacitive features of the diffusion process, without further concern about the nature of the diffusing species. In addition, constant phase elements (CPE) were used instead of capacitances, due to the non-ideal capacitive behaviour of the surface, translated in a dispersion of time constants resulting from surface heterogeneities and from uneven reactivity on the electrode surface [37]. The CPE values were converted to capacitances using the equation proposed by Brug et al. [38],

$$C = \sqrt[n]{Y_0}\left(\frac{1}{R_{series}} + \frac{1}{R_{parallel}}\right)^{\frac{n-1}{n}} \quad (4)$$

where Y_0 and n are, respectively, the frequency independent admittance and the power of the CPE, R_{series} and $R_{parallel}$ are the resistances in series and in parallel with the CPE, respectively. The evolution of the fitting parameters with time of immersion is presented in Fig. 8. Changes in C_{HF} and R_{HF} occur mainly on WC-Co and WC-FeCoNi and reflect the growth of corrosion products at the surface of the samples. The pronounced increment of C_{dl} in these two systems, reaching values much higher than the typical of a double layer (2–5 × 10^{-5} F cm^{-2}), may also be explained by the increasing amount of corrosion products (oxides and hydroxides) which, if having semiconducting properties, will extend the electrochemical active area where a double layer can be formed. The most important parameter for this work is the R_{ct}, because it is a measure of the corrosion rate. The higher the R_{ct}, the higher the resistance to corrosion. The evolution of R_{ct} observed in WC-Co suggests an increase in corrosion resistance with time, the opposite happening with WC-FeCoNi. For WC-NiCrCoMo and WC-NiCrMo, a significant increase in R_{ct} of about two orders of magnitude was measured in the two weeks testing period. This means an increased resistance to corrosion of these composites after immersion in 0.5 M NaCl.

3.2.4. Morphology of corrosion attack

Signs of corrosion were observed in WC-Co and WC-FeCoNi since the first day of immersion while no traces of attack were observed in WC-NiCrCoMo and WC-NiCrMo during the whole testing period. Figs. 9–11 show the surface of each composite after 2 weeks of immersion in 0.5 M NaCl. The optical picture of WC-Co (Fig. 9 a) presents abundant corrosion products covering the surface. Fig. 9 b) shows the surface after removing the loose corrosion products and Fig. 9 c) gives a view of the interface between part of the sample exposed to the NaCl solution and part that was protected by the adhesive tape used to delimit the exposed area. This interface is shown in more detail in d) and e) with different magnifications. The WC particles were not attacked but the binder was dissolved in part of the surface, leaving the particles detached (Fig. 9 e and f). In WC-FeCoNi the attack occurred in localised points, as pits, which appear in Fig. 10 a) surrounded by brown corrosion products. Pitting becomes more evident in Fig. 10 b) after the removal of the corrosion products. The microscopic inspection shows that the pits are covered with a cap of corrosion products. A slight abrasion of the surface reveals that most pits are shallow, with the metallic binder being dissolved and leaving the WC particles detached or weakly bonded to the bulk material.

In clear contrast with the first two composites, WC-NiCrCoMo and WC-NiCrMo did not show any signs of corrosion, as can be seen in both macroscopic and microscopic views of the surfaces – Fig. 11. White

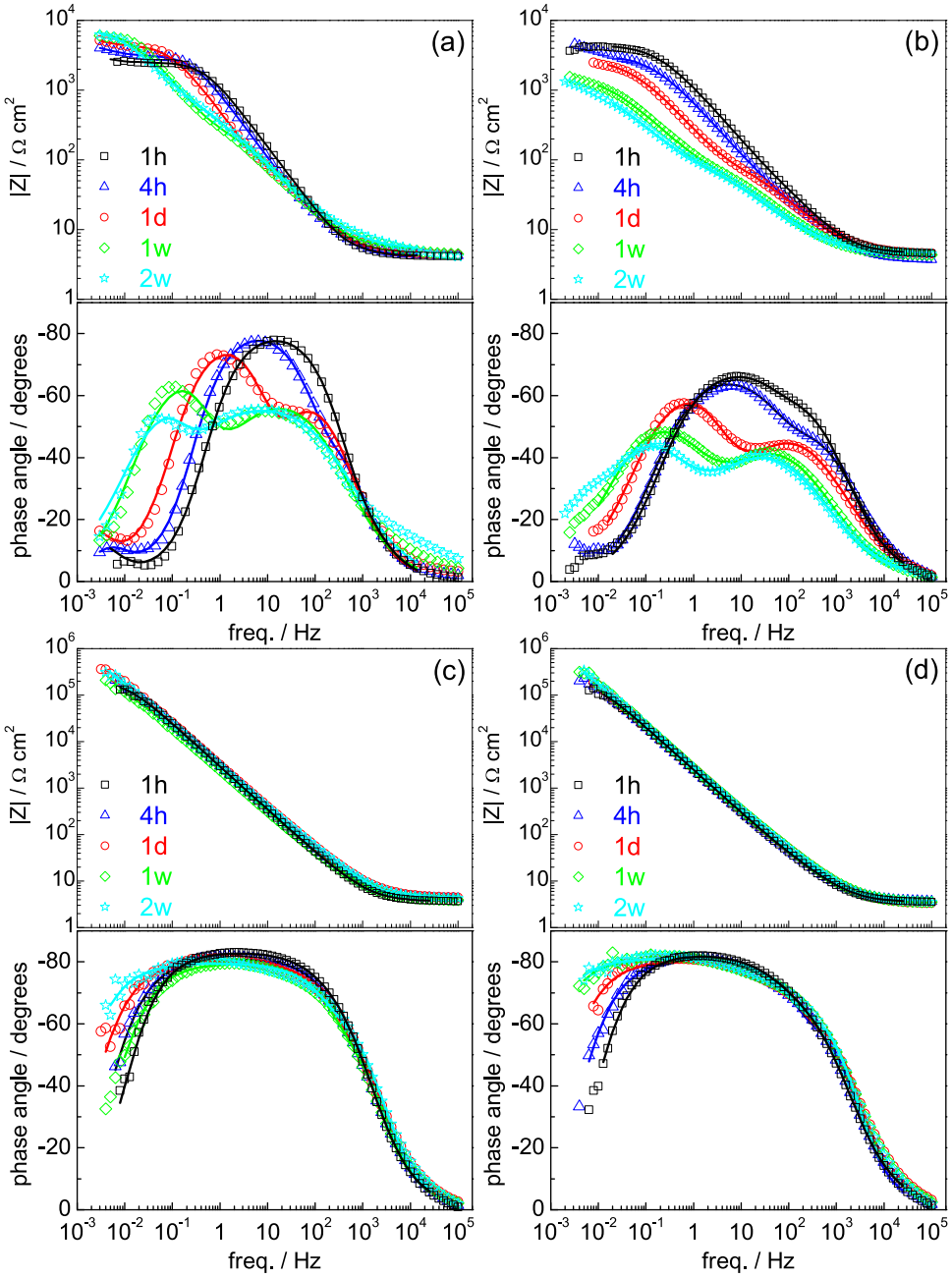

Fig. 6. Bode plots of the impedance measured in 0.5 M NaCl during 2 weeks for: (a) WC-Co, (b) WC-FeCoNi, (c) WC-NiCrCoMo and (d) WC-NiCrMo in 0.5 M NaCl. Symbols are experimental points and lines are the result of numerical fitting.

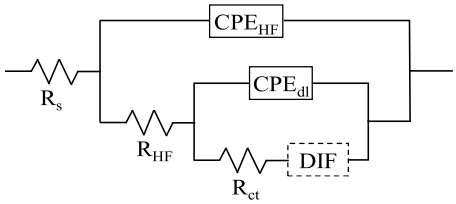

Fig. 7. Equivalent circuit used for fitting the EIS response.

points on the macroscopic images are just deposits of suspended matter in solution that remained attached to the surface after removal from solution.

3.2.5. General overview of the corrosion process

The experimental results presented in the previous sections are in line with what has been found in past studies [4,9,21,39]: in this medium the WC phase is not attacked and only the metallic binder corrodes. The oxidation of the metal phase occurs according to the reaction

$$M \rightarrow M^{n+}(aq) + ne^{-} \quad (5)$$

where M represents any metal integrating the binder. The metallic dissolution is significant in WC-Co and WC-FeCoNi but incipient for WC-NiCrCoMo and WC-NiCrMo. The cathodic reaction is mainly the reduction of dissolved O_2 according to:

$$O_2 + 2H_2O(l) + 4e^{-} \rightarrow 4OH^{-}(aq) \quad (6)$$

Following the literature, it is assumed that the cathodic activity occurs primarily in the WC grains, thus creating a galvanic couple between WC and binder, accelerating the corrosion of the latter.

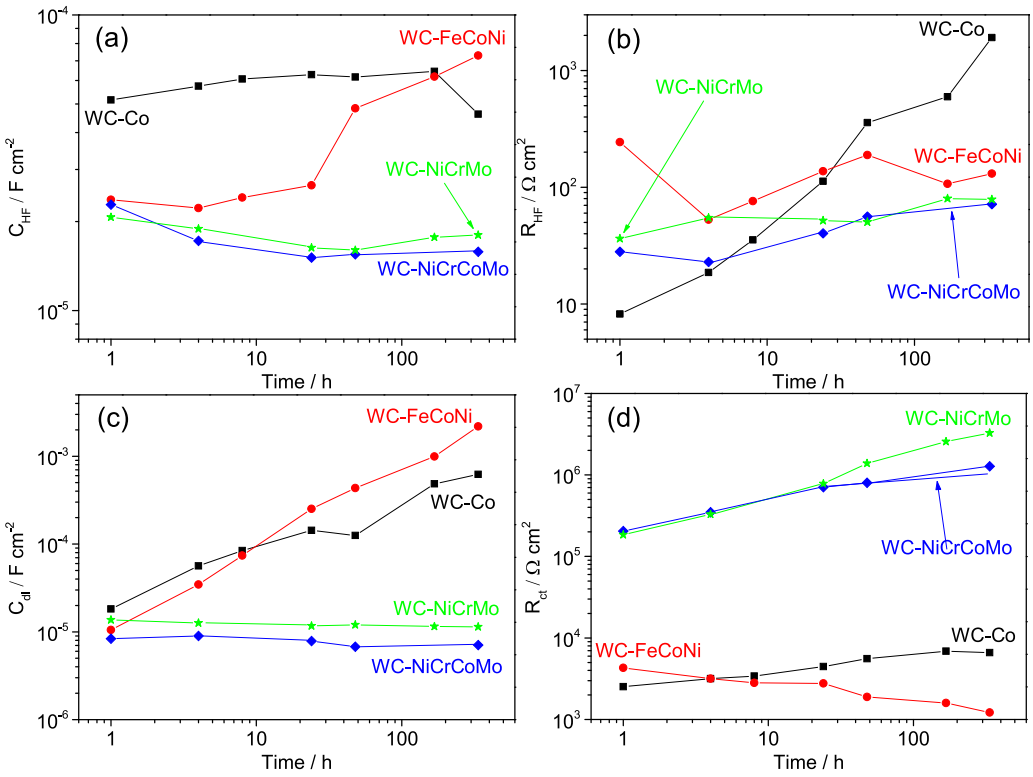

Fig. 8. Evolution of EIS fitting parameters with the time of immersion.

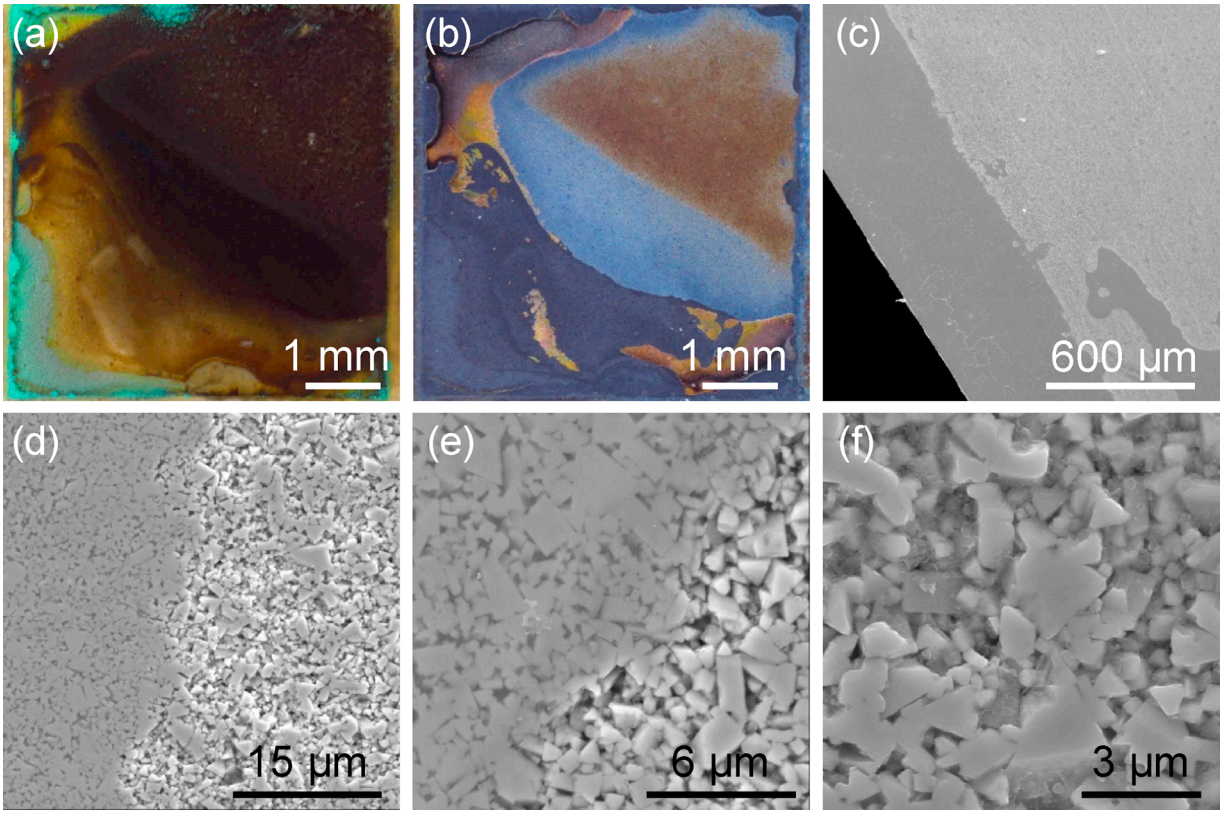

Fig. 9. Optical and SEM images of WC-Co after 2 weeks of immersion in 0.5 M NaCl.
a) surface at the end of the testing; b) same area after removal of the loose corrosion products (flushing the surface with distilled water); c) interface between the tested area and the surface protected by the adhesive tape; d) magnification of the interface; e) detail of d); f) corroded area (lack of binder surrounding the WC particles).

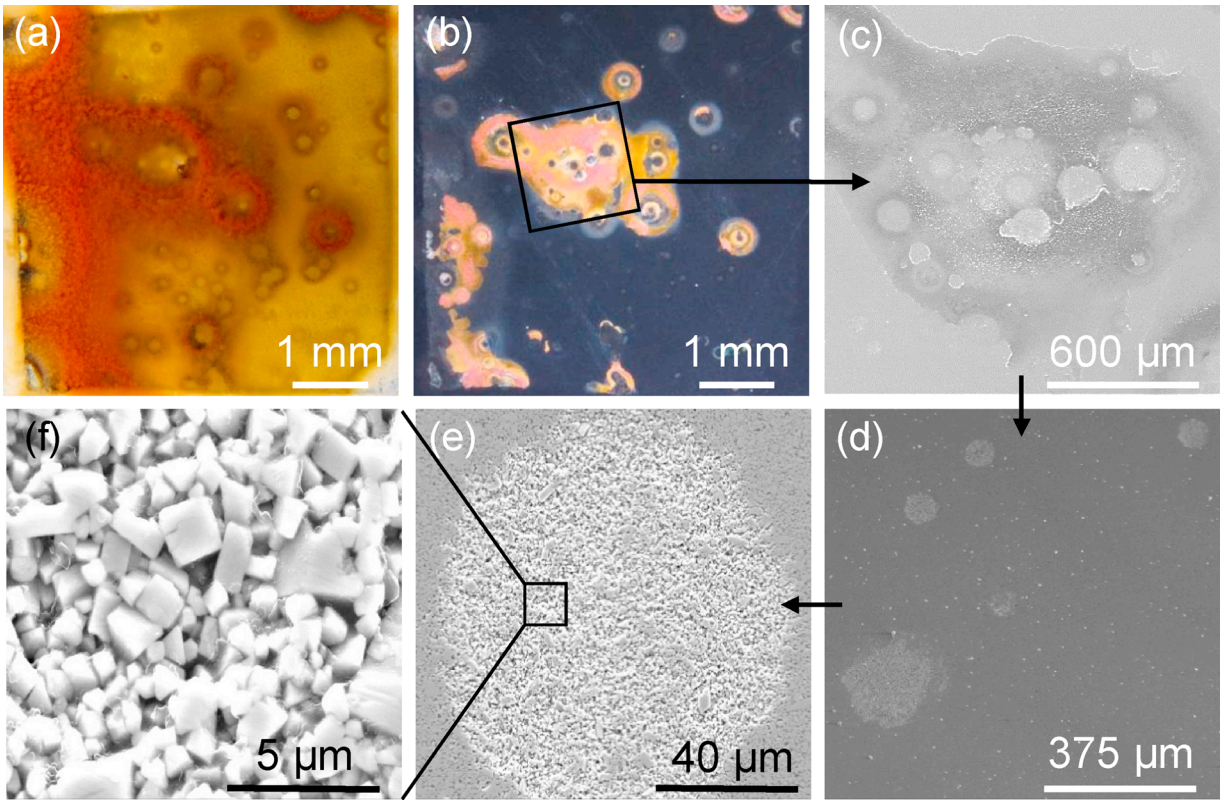

Fig. 10. Optical and SEM images of WC-FeCoNi after 2 weeks of immersion in 0.5 M NaCl: a) surface after testing; b) same area after removal of the loose corrosion products (flushing the surface with distilled water); c) magnification of a corroded region in b); d) a small area of c) after small abrasion of the surface; e) magnification of a corroded spot of d); f) inside the corroded spot (lack of binder surrounding the WC particles).

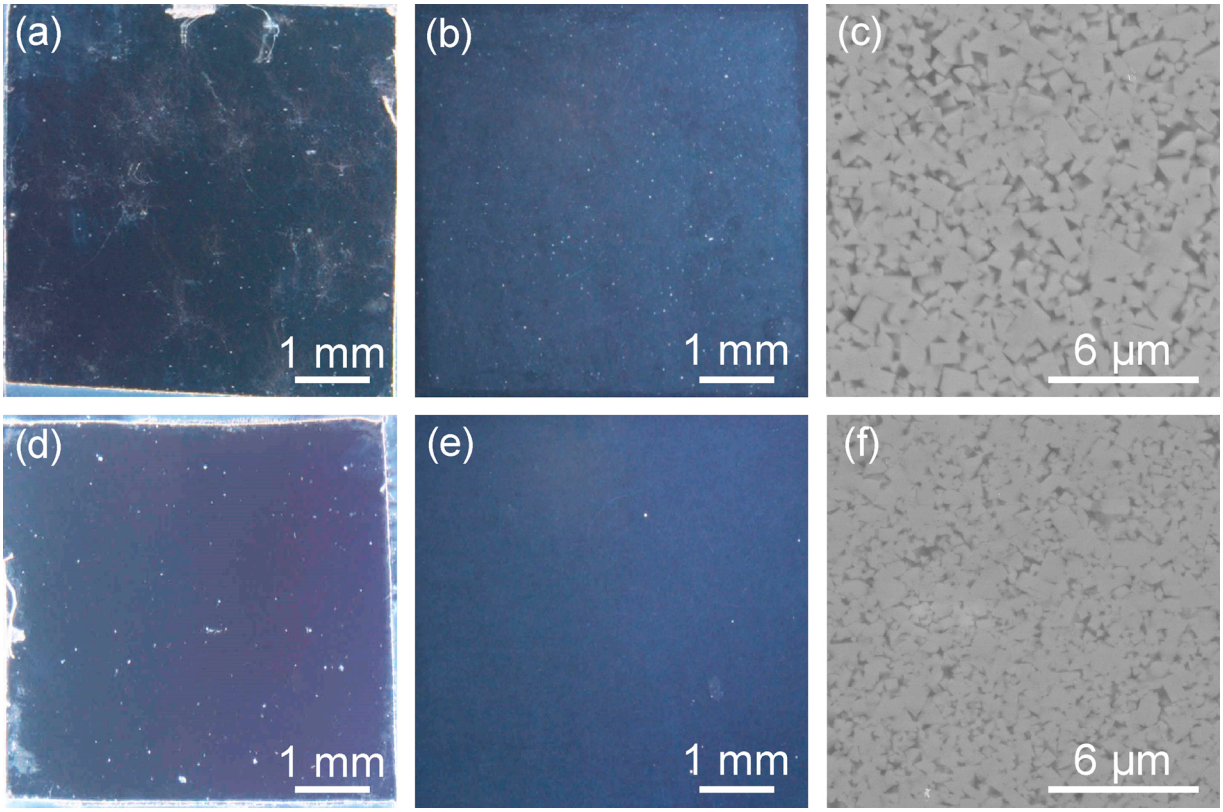

Fig. 11. Optical and SEM images of WC-NiCrCoMo (a–c) and WC-NiCrMo (d–f) after 2 weeks of immersion in 0.5 M NaCl: a) and d) surface of the samples just after testing; b) and e) same surfaces after flushing the surface with distilled water; c) and f) microscopic detail of the tested areas, showing no signs of corrosion.

The order of increasing resistance to corrosion of the studied composites is WC-Co < WC-FeCoNi < < WC-NiCrCoMo < WC-NiCrMo. This sequence follows the inverse order of the mean grain size of WC in the composites: 1 μm (WC-Co) > 0.8 μm (WC-FeCoNi) > 0.75 μm (WC-NiCrCoMo) > 0.5 μm (WC-NiCrMo). The effect of grain size on the electrochemical response of hardmetals is far from consensus. Some reports state that the smaller the grain size the higher the corrosion resistance [39–41] while other studies found no effect of grain size on the corrosion rate [4,26,42,43]. In this work the particle sizes are too similar (0.5–1 μm) to explain not only the very distinct corrosion rates but also the different corrosion patterns: general attack on WC-Co, localized in WC-FeCoNi and no corrosion on the other composites. The exposed areas of binder and WC phase are the same in all composites (18% binder/82% WC). Therefore, the determinant factor for the differences observed in this work seems to be the nature of the metallic binder and the respective resistance to corrosion. Nonetheless, the effect of particle size will be systematically studied in the future.

A final word for the corrosion resistance of WC-NiCrCoMo and WC-NiCrMo. The EIS spectra showed a capacitive behaviour typical of passive metals. No signs of corrosion were detected even after 2 weeks of immersion in 0.5 M NaCl. The anodic polarisation curves measured after 1 h of immersion depicted two regions, one close to E_{corr} with high slope, and a second region at more positive potentials where the current increased sharply. The first region can be due to a passive layer in the metal phase that grows during the time of immersion. This explains the strong increase in R_{ct} registered for these two composites during the test period. In view of this scenario, the second region can be associated to the breakdown of the passive film, with the slope in WC-NiCrCoMo similar to that of the active composites while for WC-NiCrMo a higher slope indicates a lower dissolution rate.

4. Conclusions

The alternative composites tested in this work achieved similar (WC-FeCoNi) or even higher (WC-NiCrCoMo and WC-NiCrMo) hardness than that of the WC-Co benchmark. The fracture toughness values were inside the acceptable range for this type of material. Regarding corrosion resistance, WC-FeCoNi behaved similarly to WC-Co, presenting an insufficient resistance to corrosion. Conversely, WC-NiCrCoMo and WC-NiCrMo revealed significantly higher corrosion resistance, pointing them as good replacements for WC-Co in neutral and near neutral chloride environments.

Data availability

The raw data required to reproduce these findings will be made available on request.

Acknowledgments

This work is financed by Portugal 2020 through European Regional Development Fund (ERDF) in the frame of Operational Competitiveness and Internationalization Programme (POCI) and in the scope of the project HardCorr (POCI-01-0247-FEDER-003382). The work was developed within the scope of the project CICECO-Aveiro Institute of Materials, POCI-01-0145-FEDER-007679 (FCT Ref. UID /CTM /50011/2013), financed by national funds through the FCT/MEC and when appropriate co-financed by FEDER under the PT2020 Partnership Agreement.

References

[1] H.M. Ortner, P. Ettmayer, H. Kolaska, I. Smid, The history of the technological progress of hardmetals, Int. J. Refract. Met. Hard Mater. 49 (2015) 3–8, https://doi.org/10.1016/j.ijrmhm.2014.04.016.
[2] L. Prakash, Fundamentals and general applications of hardmetals, Comprehensive Hard Materials, Elsevier, Oxford, 2014, pp. 29–90, https://doi.org/10.1016/B978-0-08-096527-7.00002-7.
[3] S.J. Park, K. Cowan, J.L. Johnson, R.M. German, Grain size measurement methods and models for nanograined WC-Co, Int. J. Refract. Met. Hard Mater. 26 (2008) 152–163, https://doi.org/10.1016/j.ijrmhm.2007.05.010.
[4] A.M. Human, H.E. Exner, Electrochemical behaviour of tungsten-carbide hardmetals, Mater. Sci. Eng. A. 209 (1996) 180–191, https://doi.org/10.1016/0921-5093(95)10137-3.
[5] D. Lison, R. Lauwerys, The interaction of cobalt metal with different carbides and other mineral particles on mouse peritoneal macrophages, Toxicol. In Vitro 9 (1995) 341–347, https://doi.org/10.1016/0887-2333(94)00211-C.
[6] C.M. Fernandes, A.M.R. Senos, Cemented carbide phase diagrams: a review, Int. J. Refract. Met. Hard Mater. 29 (2011) 405–418, https://doi.org/10.1016/j.ijrmhm.2011.02.004.
[7] C.M. Fernandes, L.M. Vilhena, C.M.S. Pinho, F.J. Oliveira, E. Soares, J. Sacramento, A.M.R. Senos, Mechanical characterization of WC-10wt% AISI 304 cemented carbides, Mater. Sci. Eng. A. 618 (2014) 629–636, https://doi.org/10.1016/j.msea.2014.09.064.
[8] N. Lin, Y. He, C. Wu, S. Liu, X. Xiao, Y. Jiang, Influence of TiC additions on the corrosion behaviour of WC – Co hardmetals in alkaline solution, RMHM 46 (2014) 52–57, https://doi.org/10.1016/j.ijrmhm.2014.05.009.
[9] S. Hochstrasser-Kurz, D. Reiss, T. Suter, C. Latkoczy, D. Günther, S. Virtanen, P.J. Uggowitzer, P. Schmutz, ICP-MS, SKPFM, XPS, and microcapillary investigation of the local corrosion mechanisms of WC–Co hardmetal, J. Electrochem. Soc. 155 (2008), https://doi.org/10.1149/1.2929822 C415.
[10] D.S. Konadu, J. van der Merwe, J.H. Potgieter, S. Potgieter-Vermaak, C.N. Machio, The corrosion behaviour of WC-VC-Co hardmetals in acidic media, Corros. Sci. 52 (2010) 3118–3125, https://doi.org/10.1016/j.corsci.2010.05.033.
[11] H. Engqvist, U. Beste, N. Axén, Influence of pH on sliding wear of WC-based materials, Int. J. Refract. Met. Hard Mater. 18 (2000) 103–109, https://doi.org/10.1016/S0263-4368(00)00007-X.
[12] E.A. Almond, B. Roebuck, Identification of optimum binder phase compositions for improved WC hard metals, Mater. Sci. Eng. A105/106 (1988) 237–248.
[13] B. Uhrenius, H. Pastor, E. Pauty, On the composition of Fe-Ni-Co-WC-based cemented carbides, Int. J. Refract. Met. Hard Mater. 15 (1997) 139–149, https://doi.org/10.1016/S0263-4368(96)00023-6.
[14] V.A. Tracey, Nickel in hardmetals, Int. J. Refract. Met. Hard Mater. 11 (1992) 137–149, https://doi.org/10.1016/0263-4368(92)90056-8.
[15] R. González, J. Echeberría, J.M. Sánchez, F. Castro, WC-(Fe,Ni,C) hardmetals with improved toughness through isothermal heat treatments, J. Mater. Sci. 30 (1995) 3435–3439, https://doi.org/10.1007/BF00349891.
[16] C.M. Fernandes, A.M.R. Senos, M.T. Vieira, J.V. Fernandes, Composites from WC powders sputter-deposited with iron rich binders, Ceram. Int. 35 (2009) 1617–1623, https://doi.org/10.1016/j.ceramint.2008.09.009.
[17] C.M. Fernandes, A.M.R. Senos, M.T. Vieira, J.M. Antunes, Mechanical characterization of composites prepared from WC powders coated with Ni rich binders, Int. J. Refract. Met. Hard Mater. 26 (2008) 491–498, https://doi.org/10.1016/j.ijrmhm.2007.12.001.
[18] M. Habibi Rad, M. Ahmadian, M.A. Golozar, Investigation of the corrosion behavior of WC-FeAl-B composites in aqueous media, Int. J. Refract. Met. Hard Mater. 35 (2012) 62–69, https://doi.org/10.1016/j.ijrmhm.2012.04.005.
[19] B.J. Marques, C.M. Fernandes, A.M.R. Senos, Sintering, microstructure and properties of WC-AISI304 powder composites, J. Alloys. Compd. 562 (2013) 164–170, https://doi.org/10.1016/j.jallcom.2013.02.013.
[20] L.M. Vilhena, C.M. Fernandes, E. Soares, J. Sacramento, A.M.R. Senos, A. Ramalho, Abrasive wear resistance of WC-Co and WC-AISI 304 composites by ball-cratering method, Wear. 346–347 (2016) 99–107, https://doi.org/10.1016/j.wear.2015.11.005.
[21] A.B. Oliveira, A.C. Bastos, C.M. Fernandes, C.M.S. Pinho, A.M.R. Senos, E. Soares, J. Sacramento, M.L. Zheludkevich, M.G.S. Ferreira, Corrosion behaviour of WC-10% AISI 304 cemented carbides, Corros. Sci. 100 (2015) 322–331, https://doi.org/10.1016/j.corsci.2015.08.006.
[22] C.M. Fernandes, A. Rocha, J.P. Cardoso, A.C. Bastos, E. Soares, J. Sacramento, M.G.S. Ferreira, A.M.R. Senos, WC-stainless steel hardmetals, Int. J. Refract. Met. Hard Mater. 72 (2018) 21–26, https://doi.org/10.1016/j.ijrmhm.2017.11.046.
[23] V. Bounhoure, S. Lay, S. Coindeau, S. Norgren, E. Pauty, J.M. Missiaen, Effect of Cr addition on solid state sintering of WC-Co alloys, Int. J. Refract. Met. Hard Mater. 52 (2015), https://doi.org/10.1016/j.ijrmhm.2015.05.002.
[24] H. Scholl, B. Hofman, A. Rauscher, Anodic polarization of cemented carbides of the type [(WC,M): M = Fe, Ni or Co] in sulphuric acid solution, Electrochim. Acta 37 (1992) 447–452, https://doi.org/10.1016/0013-4686(92)87034-W.
[25] N. Lin, C.H. Wu, Y.H. He, D.F. Zhang, Effect of Mo and Co additions on the microstructure and properties of WC-TiC-Ni cemented carbides, Int. J. Refract. Met. Hard Mater. 30 (2012) 107–113, https://doi.org/10.1016/j.ijrmhm.2011.07.011.
[26] W.J. Tomlinson, C.R. Linzell, Anodic polarization and corrosion of cemented carbides with cobalt and nickel binders, J. Mater. Sci. 23 (1988) 914–918, https://doi.org/10.1007/BF01153988.
[27] W. Callister, D. Rethwisch, Materials Science and Engineering: an Introduction, (2007), https://doi.org/10.1016/0025-5416(87)90343-0.
[28] ImageJ (http:/imagej.nih.gov/ij/, last view on January 31st, 2018).
[29] D.K. Shetty, I.G. Wright, P.N. Mincer, A.H. Clauer, Indentation fracture of WC-Co cermets, J. Mater. Sci. 20 (1985) 1873–1882.
[30] W.D. Schubert, H. Neumeister, G. Kinger, B. Lux, Hardness to toughness relationship of fine-grained WC-Co hardmetals, Int. J. Refract. Met. Hard Mater. 16 (1998) 133–142, https://doi.org/10.1016/S0263-4368(98)00028-6.
[31] P. Ettmayer, H. Kolaska, H.M. Ortner, 1.01 – history of hardmetals, Comprehensive

Hard Materials, Elsevier, Oxford, 2014, pp. 4–27, https://doi.org/10.1016/B978-0-08-096527-7.00001-5.
[32] M. Aristizabal, L.C. Ardila, F. Veiga, M. Arizmendi, J. Fernandez, J.M. Sánchez, Comparison of the friction and wear behaviour of WC – Ni – Co – Cr and WC – Co hardmetals in contact with steel at high temperatures, Wear 280–281 (2012) 15–21, https://doi.org/10.1016/j.wear.2012.01.015.
[33] V. Richter, M. Ruthendorf, On hardness and toughness of ultrafine and nanocrystalline hard materials, Int. J. Refract. Metals Hard Mater. 17 (1999) 141–152.
[34] L. Zhang, S. Chen, C. Shan, X. Cheng, Y. Ma, X.-J. Xiong, Effects of cobalt additions on WC grain growth, Powder Metall. 55 (2012) 200–205, https://doi.org/10.1179/1743290111Y.0000000009.
[35] M. Stern, Electrochemical polarization - I. A theoretical analysis of the shape of polarization curves, J. Electrochem. Soc. 104 (1957) 559, https://doi.org/10.1149/1.2428653.
[36] Einar Bardal, Corrosion and Protection, Springer, 2004, https://doi.org/10.1007/b97510.
[37] M.E. Orazem, B. Tribollet, Electrochemical Impedance Spectroscopy, (2008), https://doi.org/10.1002/9780470381588.
[38] G.J. Brug, A.L.G. van den Eeden, M. Sluyters-Rehbach, J.H. Sluyters, The analysis of electrode impedances complicated by the presence of a constant phase element, J. Electroanal. Chem. Lausanne (Lausanne) 176 (1984) 275–295, https://doi.org/10.1016/S0022-0728(84)80324-1.
[39] S.H. Kurz, Y. Mueller, C. Latkoczy, S. Virtanen, P. Schmutz, Analytical characterization of the corrosion mechanisms of WC–Co by electrochemical methods and inductively coupled plasma mass spectroscopy, Corros. Sci. 49 (2007) 2002–2020.
[40] F.J.J. Kellner, H. Hildebrand, S. Virtanen, Effect of WC grain size on the corrosion behavior of WC–Co based hardmetals in alkaline solutions, Int. J. Refract. Met. Hard Mater. 27 (2009) 806.
[41] W.J. Tomlinson, N.J. Ayerst, Anodic polarization and corrosion of WC–Co hardmetals containing small amounts of Cr3Ca and/or VC, J. Mater. Sci. 24 (1989) 2348.
[42] A.M. Human, H.E. Exner, The relationship between electrochemical behaviour and in-service corrosion of WC based cemented carbides, Int. J. Refract. Met. Hard Mater. 15 (1997) 65.
[43] Q. Zhang, N. Lin, Y. He, Effects of Mo additions on the corrosion behavior of WC-TiC-Ni hardmetals in acidic solutions, Int. J. Refract. Met. Hard Mater. 38 (2013) 15.